Journal of Environmental Chemical Engineering 10 (2022) 107467

Contents lists available at ScienceDirect

Journal of Environmental Chemical Engineering

journal homepage: www.elsevier.com/locate/jece

Magnetic metal-organic frameworks for efficient removal of cadmium(II), and lead(II) from aqueous solution

Ahmed F. Abdel-Magied [a,b,**,1], Hani Nasser Abdelhamid [c,d,***,1], Radwa M. Ashour [a,b], Le Fu [e], Moataz Dowaidar [f], Wei Xia [g], Kerstin Forsberg [a,*]

[a] Department of Chemical Engineering, KTH Royal Institute of Technology, 100 44 Stockholm, Sweden
[b] Nuclear Materials Authority, P. O. Box 530, El Maadi, Cairo, Egypt
[c] Advanced Multifunctional Materials Laboratory, Department of Chemistry, Assiut University, 71515, Assiut, Egypt
[d] Department of Materials and Environmental Chemistry, Stockholm University, Stockholm SE-10691, Sweden
[e] School of Materials Science and Engineering, Central South University, Changsha, Hunan 410083, China
[f] Department of Bioengineering, King Fahd University of Petroleum and Minerals (KFUPM), Dhahran 31261, Saudi Arabia
[g] Department of Materials Science and Engineering, Uppsala University, Uppsala, Sweden

ARTICLE INFO

Editor: Despo Kassinos

Keywords:
Metal organic frameworks (MOFs)
Adsorption
Magnetic nanoparticles
Cadmium ion (Cd)
Lead ion (Pb)

ABSTRACT

Efficient and convenient methods for the removal of toxic heavy metal ions especially Cd(II) and Pb(II) from aqueous solutions is of great importance due to their serious threat to public health and the ecological system. In this study, two magnetic metal-organic frameworks (namely: Fe_3O_4@ZIF-8, and Fe_3O_4@UiO-66–NH_2) were synthesized, fully characterized, and applied for the adsorption of Cd(II) and Pb(II) from aqueous solutions. The adsorption efficiencies for the prepared nanocomposites are strongly dependent on the pH of the aqueous solution. The maximum adsorption capacities of Fe_3O_4@UiO-66–NH_2, and Fe_3O_4@ZIF-8 at pH 6.0 were calculated to be 714.3 mg·g^{-}, and 370 mg·g^{-1} for Cd(II), respectively, and 833.3 mg·g^{-1}, and 666.7 mg·g^{-1} for Pb(II), respectively. The adsorption process follows a *pseudo*-second-order model and fit the Langmuir isotherm model. Moreover, the thermodynamic studies revealed that the adsorption process is endothermic, and spontaneous in nature. A plausible adsorption mechanism was discussed in detail. The magnetic adsorbents: Fe_3O_4@ZIF-8, and Fe_3O_4@UiO-66–NH_2 showed excellent reusability, maintaining the same efficiency for at least four consecutive cycles. These results reveal the potential use of magnetic Fe_3O_4@ZIF-8, and Fe_3O_4@UiO-66–NH_2 as efficient adsorbents in removing Cd(II) and Pb(II) from aqueous solutions.

1. Introduction

Over the last decade, numerous environmental pollutants have been released into the environment due to the accelerating pace of industrialization [1,2]. Among environmental contaminants, toxic heavy metal ions are considered as a collection of hazardous and destructive pollutants [3]. Due to their high solubility, they are easily absorbed by aquatic species, resulting in increased concentration [4]. Toxic heavy metals such as cadmium (Cd) and lead (Pb) have a long biological half-life of 7–16 years and 150 years in the human body, respectively, and can cause harmful effects [5,6]. Various techniques for the removal of Cd(II) and Pb(II) from aqueous solutions including precipitation [7], membrane [8], ion-exchange [9], solid phase extraction [10], phytoremediation [11], and electrochemical based methods [12], have been investigated over the last decades, however, these techniques have various disadvantages such as special working conditions, and complex contaminants removal processes. In contrast, adsorption techniques for the removal of contaminates from aqueous solutions stands out considering its valuable properties such as high efficiency, simple design, easy regeneration, good selectivity, and low operational cost [13,14]. Many adsorbents including molybdenum disulfide nanosheets decorated with cerium oxide nanoparticles [15], biomass [16], magnetic

* Corresponding author.
** Corresponding author at: Department of Chemical Engineering, KTH Royal Institute of Technology, 100 44 Stockholm, Sweden.
*** Corresponding author at: Advanced Multifunctional Materials Laboratory, Department of Chemistry, Assiut University, 71515, Assiut, Egypt.
E-mail addresses: fawzy@kth.se (A.F. Abdel-Magied), hany.abdelhamid@aun.edu.eg (H.N. Abdelhamid), kerstino@kth.se (K. Forsberg).
[1] These authors contributed equally to this work

https://doi.org/10.1016/j.jece.2022.107467
Received 30 November 2021; Received in revised form 7 February 2022; Accepted 23 February 2022
Available online 24 February 2022

nanoparticles [17], and polymers [18], have been extensively investigated for the removal of Cd(II) or Pb(II) from aqueous solutions; however, these materials usually suffer from low removal efficiencies or low adsorption capacities, which have largely limited their effectiveness. Furthermore, they require a tedious process for separation and lack of recyclability [19]. Recently, metal-organic frameworks (MOFs) have been explored for the removal of heavy metal ions from aqueous solutions, due to their many attractive characteristics, such as high surface area, large pores, high chemical, and solvent stability [20–23]. However, MOFs separation after the adsorption process is still a challenge due to the need to use a filter or centrifuge [20]. Therefore, an easier separable design of MOFs adsorbents for the removal of heavy metal ions contaminants from aqueous solutions, that can overcome the weakness associated with the existing adsorbents, is essential for widespread applications. Magnetic MOFs have received considerable interest in contaminants removals since they can easily be separated from the aqueous solutions using an external magnet field, thus avoiding extra experimental steps, such as filtration of centrifugation [24,25]. Composite MOF materials show great promise for many applications however their synthesis can be challenging, especially when considering process scale up [26]. The method chosen should produce a material of sufficient quality for the specific application.

In this work, we report the synthesis and full characterization of two magnetic nanocomposites, namely Fe_3O_4@ZIF-8 (zeolitic imidazolate frameworks-8) [27] and Fe_3O_4@UiO-66–NH_2 (UiO refers to university in Oslo) [28]. The synthesized magnetic nanoparticles Fe_3O_4@ZIF-8 and Fe_3O_4@UiO-66–NH_2 offer high adsorption efficiencies for Cd(II), and Pb (II) from aqueous solutions. The influence of key factors to be able to design an efficient adsorption process, including, pH value of the metal solution, adsorption contact time, adsorption capacity, effect of temperature, and adsorbent recyclability were investigated. Furthermore, kinetics, thermodynamics, and the mechanisms of the adsorption processes were discussed.

2. Experimental

2.1. Chemicals and reagents

Lead chloride ($PbCl_2$, 98%), cadmium nitrate tetrahydrate ($Cd(NO_3)_2{\cdot}4\ H_2O$, 98%), sodium hydroxide (NaOH, ≥ 98%), iron sulfate ($FeSO_4{\cdot}7\ H_2O$, ≥ 99%), iron nitrate ($Fe(NO_3)_3{\cdot}9\ H_2O$, ≥ 98%), zinc nitrate ($Zn(NO_3)_2{\cdot}6\ H_2O$, 98%), 2-aminoterephthalic acid (BDC-NH_2, 99%), 2-methylimidazole (Hmim, 99%), triethylamine (TEA, ≥ 99%), acetic acid (≥ 99%), dimethyl formamide (DMF, ≥ 99.9%), $ZrCl_4$ (≥ 99.5%), methanol (≥ 99.8%), and nitric acid (HNO_3, 69%) were purchased from Sigma Aldrich (Germany). All the chemical reagents were used without further purification. Doubly distilled water was used throughout the experiments.

2.2. Synthesis of the magnetic Fe_3O_4@ZIF-8 and Fe_3O_4@UiO-66–NH_2 nanocomposites

The magnetic nanoparticles were synthesized using a co-precipitation method with a slight modification [29–31]. Typically, an aqueous solution of $FeSO_4$ (0.63 g) and $Fe(NO_3)_3$ (1.73 g) were prepared using deionized water (25 mL). Then a solution of NH_4OH (25 mL, 30%) was added and the solution was left for 1 h at 90 °C. The synthesized magnetic nanoparticles were separated using an external magnet. The materials were washed several times using deionized water (2 ×30 mL). The magnetic nanoparticles were then again collected using an external magnet and the samples were dried under vacuum at 85 °C overnight.

UiO-66-NH_2 material was synthesized using a solvothermal method with modifications [32]. First, $ZrCl_4$ (37 mmol) and BDC-NH_2 (33 mmol) were dissolved in acetic acid (10 mL) and DMF (25 mL). The reaction container was heated at 120 °C for 24 h. Subsequently, the product was collected via centrifugation (12000 rpm), washed three times with DMF, and soaked in methanol at 60 °C for three days with replacing the soaking solvent every 24 h to exchange DMF, and finally dried at 100 °C overnight.

Zeolitic imidazolate framework (ZIF-8) particles are synthesized according to our previously reported procedure [33]. Briefly, in a glass scintillation vial, TEA (0.70 mmol) was added to $Zn(NO_3)_2{\cdot}6\ H_2O$ solution (0.67 mmol) followed by addition of 2.3 mL of the Hmim solution (48.0 mmol). The reaction mixture was stirred for 30 min. The product was collected using centrifugation (12000 rpm). The materials were washed several times using deionized water (3 ×50 mL), and finally dried at 85 °C overnight.

The magnetic nanocomposites Fe_3O_4@ZIF–8 and Fe_3O_4@UiO–66–NH_2 were prepared using ultrasonication. Typically, 0.5 g of magnetic nanoparticles were dispersed in 50 mL methanol. UiO–66–NH_2 and ZIF–8 (0.5 g) were added under ultrasonication for 5 min. The final prepared magnetic nanocomposites Fe_3O_4@ZIF–8 and Fe_3O_4@UiO–66–NH_2 were separated from the methanol solution using an external magnet. The collected materials were washed using deionized water (2 ×50 mL) and dried at 60 °C for 12 h.

2.3. Characterization of materials

The phases of the formed materials were identified using X-ray diffraction (PANanalytical X'Pert PRO diffractometer coupled with Cu $K_{\alpha1}$ radiation, λ = 1.5406 Å. The morphology and particle size of Fe_3O_4@ZIF–8 and Fe_3O_4@UiO–66–NH_2 were investigated using transmission electron microscopy (TEM, TEM-2100, JEOL, Japan, accelerating voltage 200 kV. Scanning Electron Microscope (SEM) and Energy Dispersive X-ray (EDX) for elemental analysis and mapping were measured using TM-3000 (Hitachi). N_2 adsorption−desorption isotherms (77 K) were recorded using a Micromeritics ASAP 2020 (Micromeritics Ltd., England). The samples were evacuated at 120 °C for 3 h in vacuum before measurement. The pore volumes were calculated at P/P_0 of 0.98 of the N_2 sorption isotherms at 77 K. The pore size, the micropore volumes and external surface area were calculated using the t-plot method. Pore size distribution of the materials was determined using a DFT method [34]. The total concentrations of metal ions were determined by inductively coupled plasma optical emission spectrometry (ICP-OES, Thermo Fisher iCAP 7400, USA). The pH value of the solution was measured by a pH-meter (ORION Star A211, Thermo-Scientific™, USA). Zeta potential of Fe_3O_4@ZIF-8 and Fe_3O_4@UiO–66–NH_2 were determined using a Zetasizer Nano ZS (Malvern, UK). The elemental composition of samples and information about the bonding environment was obtained by X-ray photoelectron spectroscopy (XPS, Physical Electronics Quantum 2000, Al K_α X-ray source). Powder samples were spread and adhered on adhesive carbon tape. The spectral energies were calibrated by setting the binding energy of the C—C as a reference at 285.0 eV. Data analysis was performed using the MultiPak software (Physical Electronics).

2.4. Batch adsorption experiments

Stock solutions of Cd(II) and Pb(II) were prepared using $Cd(NO_3)_2{\cdot}4\ H_2O$ and $PbCl_2$ salts. The pH of the stock solutions was adjusted using NaOH (0.1 M) and HCl (0.1 M). Adsorption experiments were carried out by adding the desired dosage of Fe_3O_4@ZIF-8 and Fe_3O_4@UiO-66-NH_2 to 10 mL of Cd(II) and Pb(II) solutions at a given concentration and the suspensions were stirred at a constant speed of 300 rpm for a certain amount of time. The magnetic framework composites Fe_3O_4@ZIF-8 and Fe_3O_4@UiO-66-NH_2 were separated from the aqueous solution with an external magnet, and the concentration of Cd(II) and Pb(II) in the supernatant was determined using ICP-OES. The adsorption capacity (q_e, $mg{\cdot}g^{-1}$), and the removal percentage (%) were calculated as follows:

$$q_e = \frac{(C_0 - C_e)V}{m} \quad (1)$$

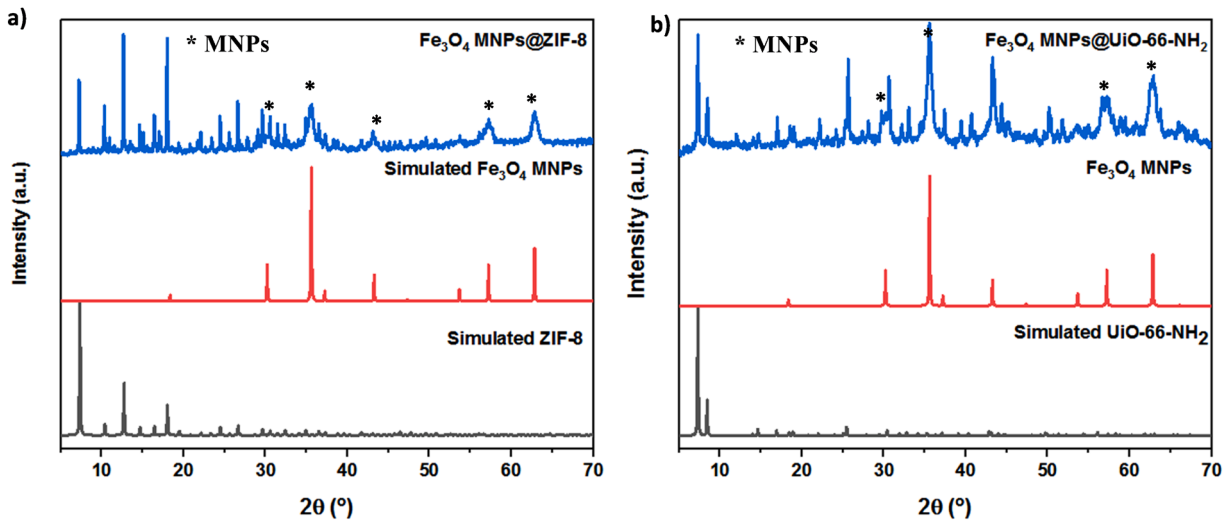

Fig. 1. XRD patterns for a) Fe_3O_4@ZIF-8, and b) Fe_3O_4@UiO-66–NH_2.

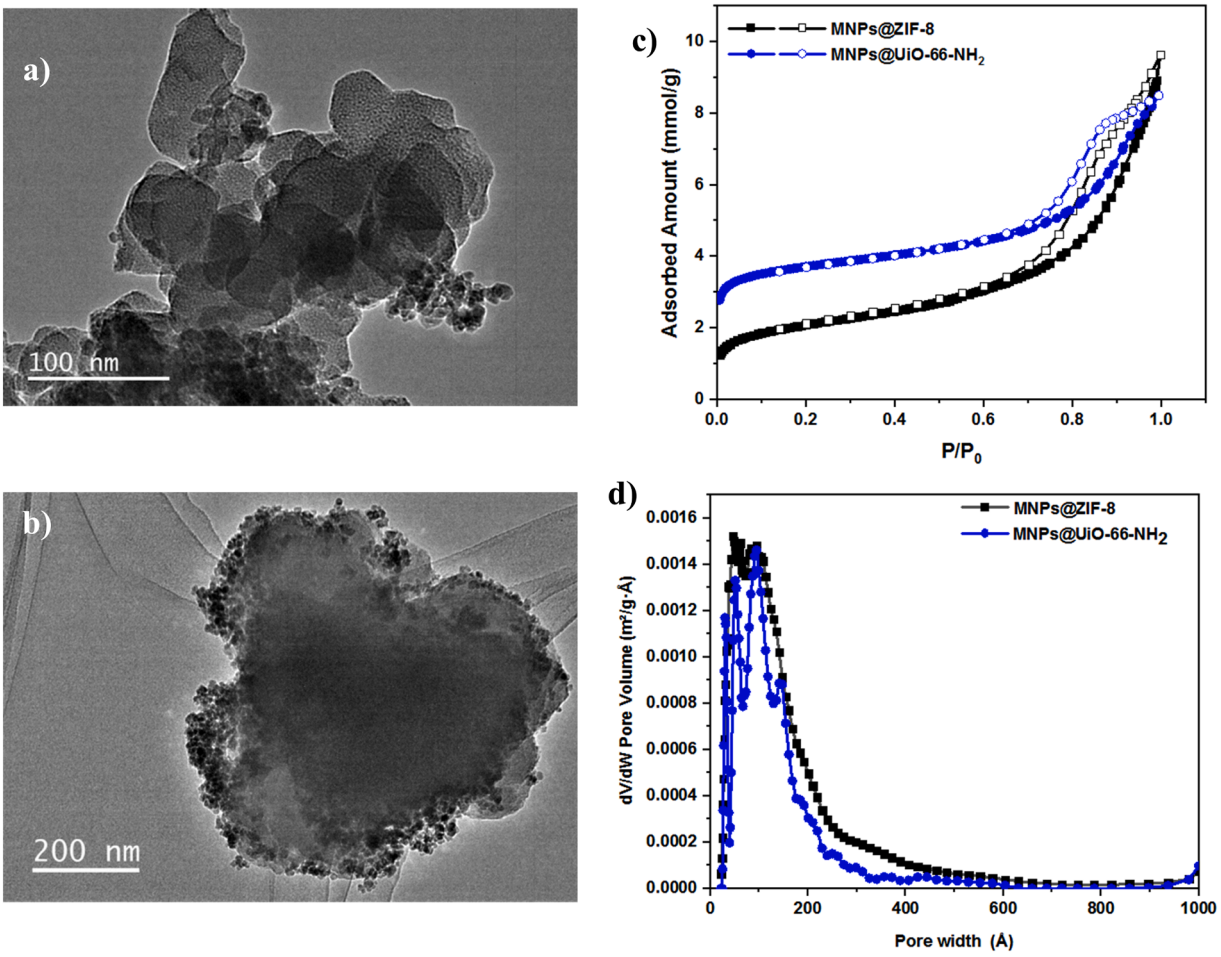

Fig. 2. TEM images for a) Fe_3O_4@ZIF-8, and b) Fe_3O_4@UiO-66–NH_2, c) N_2 adsorption-desorption isotherms, and d) Pore size distribution using DFT.

$$\text{Removal}(\%) = \frac{(C_0 - C_e)}{C_0} \times 100 \quad (2)$$

where C_0 and C_e ($mg{\cdot}L^{-1}$) are the initial and equilibrium concentration in aqueous solution, respectively, V (mL) is the volume of the aqueous phase, and m (g) is the mass of adsorbent. The adsorption experiments were performed in duplicate/triplicate and the average values of total adsorption are reported, with relative errors less than 5%.

2.5. Desorption experiments

The regeneration and recyclability of the Fe_3O_4@ZIF-8 and

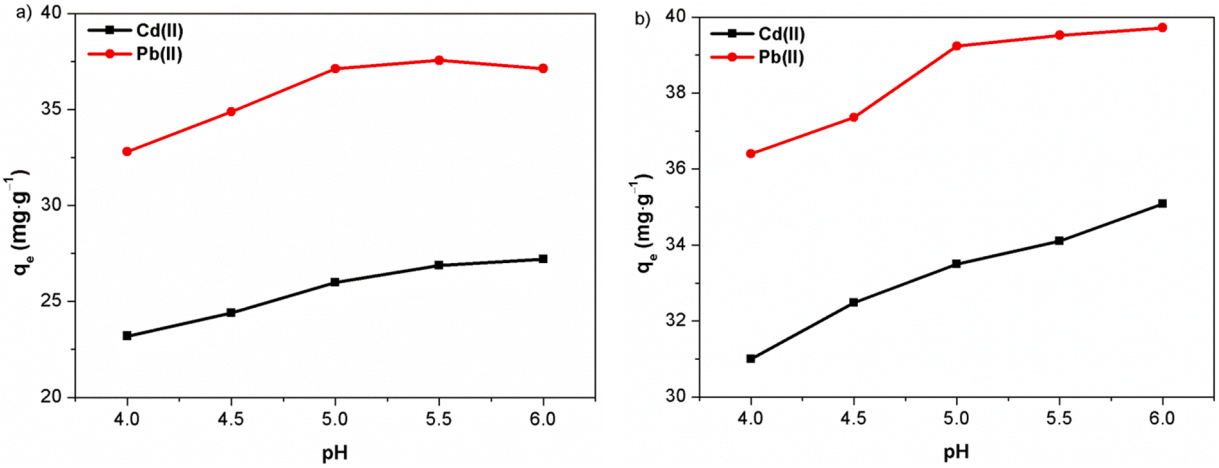

Fig. 3. Effect of initial solution pH on the adsorption capacities for Cd(II) and Pb(II) using (a) Fe_3O_4@ZIF-8, and (b) Fe_3O_4@UiO-66–NH_2. Experimental conditions: C_0 = 10 mg·L^{-1}, Fe_3O_4@ZIF-8, and Fe_3O_4@UiO-66–NH_2 = 2.5 mg, V = 10 mL, time = 24 h at room temperature.

Fe_3O_4@UiO-66–NH_2 after adsorption of Cd(II) and Pb(II) was evaluated. To regenerate the materials, the loaded Fe_3O_4@ZIF-8 and Fe_3O_4@UiO-66–NH_2 were stirred in acetonitrile solution for 10 h, then separated from the aqueous solution via an external magnet, and finally dried at 85 °C overnight in an oven for the next usage.

3. Results and discussion

3.1. Characterization of Fe_3O_4@ZIF-8 and Fe_3O_4@UiO-66–NH_2

Two MOFs, UiO-66–NH_2, and ZIF-8, were used to be conjugated with Fe_3O_4 magnetic nanoparticles (MNPs). The phases of the materials were identified by XRD (Fig. 1). The collected data showed that the XRD patterns of the prepared materials are in good agreement with the simulated pattern, confirming the formation of ZIF-8, and UiO-66–NH_2. The XRD patterns show no extra phases and confirm that the materials have high purity. The XRD for the prepared Fe_3O_4@ZIF-8 shows high stability after soaking in water for 3 days (Fig. S1). The morphology and particle size of the formed composite was evaluated using TEM (Fig. (2a-b)). TEM images show distribution of magnetic nanoparticles on the crystal surfaces of ZIF-8 and UiO-66–NH_2. Porosity of the materials was determined using N_2 adsorption-desorption isotherms (Fig. 2(c-d), Table S1). The collected data showed Brunauer–Emmett–Teller (BET) specific surface area of 160 $m^2 \cdot g^{-1}$, and 287 $m^2 \cdot g^{-1}$ for Fe_3O_4@ZIF-8 and Fe_3O_4@UiO-66–NH_2, respectively. The Langmuir surface areas were determined to be 213 $m^2 \cdot g^{-1}$, and 368 $m^2 \cdot g^{-1}$ for Fe_3O_4@ZIF-8 and Fe_3O_4@UiO-66−NH_2, respectively. The analysis reveals an external surface area of 116 $m^2 \cdot g^{-1}$, and 103 $m^2 \cdot g^{-1}$ with pore volume of 0.33 and 0.29 $cm^3 \cdot g^{-1}$ for Fe_3O_4@ZIF-8 and Fe_3O_4@UiO-66−NH_2, respectively (Table S1). Pore size distribution shows the presence of mesopores with pore volume of 0.21–0.31 $cm^3 \cdot g^{-1}$ that were created due to the interparticle pore between MOFs and MNPs, as can be seen in the TEM images (Fig. 2(d)). SEM image and EDX analysis of the prepared composites Fe_3O_4@ZIF-8 and Fe_3O_4@UiO-66–NH_2 are shown in Fig. S2, and S3, respectively. The FT-IR spectra for UiO-66-NH_2, ZIF-8, Fe_3O_4 MNPs, and their magnetic nanocomposite are shown in Figure S4. They showed characteristic bands at a wavenumber of 541 cm^{-1} corresponding to Fe-O bond. The FT-IR spectrum of UiO-66-NH_2 shows characteristic bands at wavenumber the peak at 751 cm^{-1} that can be assigned to the symmetric vibration of O-Zr-O. The FT-IR spectrum of ZIF-8 displays a characteristic band at 421 cm^{-1} corresponding to the Zn-N bond [35, 36]. The spectra of the composite show the characteristic feature of both components.

3.2. Effect of initial pH on Cd(II) and Pb(II) removal

The adsorption of metal ions onto Fe_3O_4@ZIF-8, and Fe_3O_4@UiO-66–NH_2 are strongly dependent on solution pH and the Zeta potential of the materials. The adsorption of Cd(II), and Pb(II) was studied for initial pH values in the range of 4–6. Cadmium and lead will precipitate at pH > 8 and > 6, respectively [37], moreover, the structure of Fe_3O_4@ZIF-8 in aqueous solutions is only stable at pH > 2.5 [25]. The effect of pH value on the competitive adsorption capacity of Cd(II), and Pb(II) using Fe_3O_4@ZIF-8 and Fe_3O_4@UiO-66-NH_2 is shown in Fig. 3(a) and (b), respectively, and the removal percentage for Cd(II) and Pb(II) using Fe_3O_4@ZIF-8 and Fe_3O_4@UiO-66–NH_2 is shown in Fig. S5(a) and (b), respectively. As expected, the pH had a significant influence on the adsorption capacity of Cd(II) and Pb(II) onto Fe_3O_4@ZIF-8, and Fe_3O_4@UiO-66-NH_2. At higher pH values, higher adsorption capacities for Cd(II) and Pb(II) were obtained. Such behavior can be attributed to the isoelectric point (IEP) for Fe_3O_4@ZIF-8, and Fe_3O_4@UiO-66–NH_2 as shown in Fig. S6. The measured IEP values for Fe_3O_4@ZIF-8, and Fe_3O_4@UiO-66–NH_2 were 5.01 and 4.98, respectively. When the pH of the solution is higher than the IEP, the magnetic MOFs composites surface is negatively charged, and this may enhance the electrostatic interactions between Cd(II) and Pb(II) and Fe_3O_4@ZIF-8, and Fe_3O_4@UiO-66–NH_2, leading to higher adsorption capacities. On the contrary, at lower pH values (pH<IEP), the surface charge of Fe_3O_4@-ZIF-8, and Fe_3O_4@UiO-66-NH_2 is positive, restricting the approach of Cd(II) and Pb(II), leading to low adsorption capacities. The effect of pH on the adsorption of Cd(II) and Pb(II) is in agreement with previously reported findings [38,39]. In consideration of high adsorption capacities, pH 6 was selected for subsequent studies.

3.3. Adsorption kinetics

The effect of contact time on the competitive adsorption of Cd(II) and Pb(II) onto Fe_3O_4@ZIF-8, and Fe_3O_4@UiO-66–NH_2 is presented in Fig. S7(a) and (b), respectively. A series of identical experiments were carried out varying the contact time (5 min−24 h). The adsorption amount (q_t, mg·g^{-1}) increased rapidly in the first 2 h and about 87% of Cd(II) and 79% of Pb(II) can be adsorbed in case of Fe_3O_4@ZIF-8, while for Fe_3O_4@UiO-66–NH_2, 76% of Cd(II) and 77% of Pb(II) were adsorbed. Then, for adsorption onto Fe_3O_4@ZIF-8 equilibrium is reached after 5 h for the adsorption of Cd(II) reaching a q_e of 27 mg·g^{-1}, and after 8 h for adsorption of Pb(II), reaching a q_e of 37 mg·g^{-1}. In case of Fe_3O_4@UiO-66-NH_2, 35 mg·g^{-1} of Cd(II) and 40 mg·g^{-1}of Pb(II) were absorbed after 5 and 8 h, respectively.

To describe the kinetics of Cd(II) and Pb(II) adsorption on the

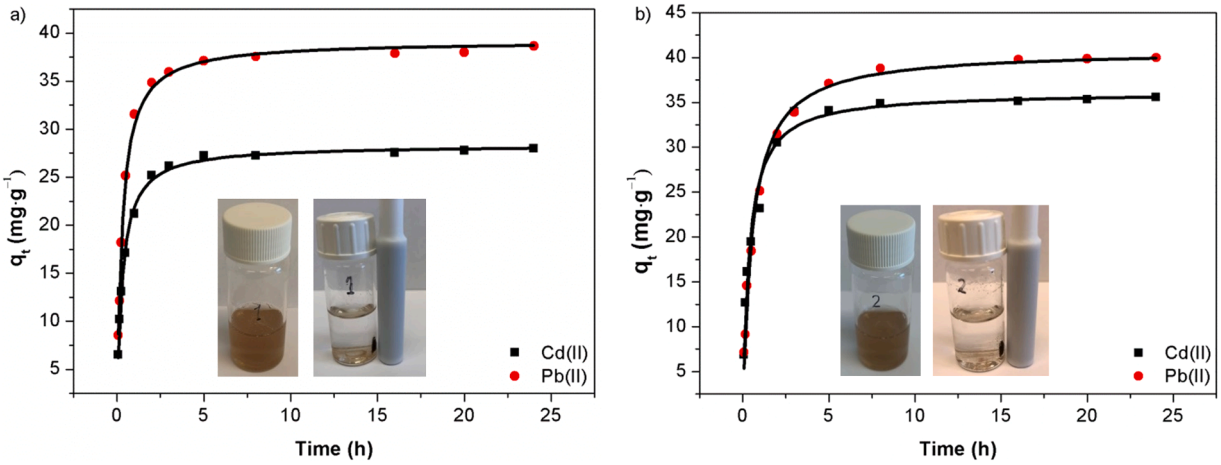

Fig. 4. Pseudo-second-order kinetic models for the adsorption of Cd(II) and Pb(II) using (a) Fe_3O_4@ZIF-8, and (b) Fe_3O_4@UiO-66–NH_2. Experimental conditions: C_0 = 10 mg·L^{-1}, MFCs (Fe_3O_4@ZIF-8, and Fe_3O_4@UiO-66–NH_2) = 2.5 mg, V = 10 mL, pH = 6 at room temperature.

Table 1
Kinetic and modeling of Cd(II) and Pb(II) adsorption onto Fe_3O_4@ZIF-8 and Fe_3O_4@UiO-66–NH_2 using pseudo-first-order and Pseudo-second-order models.

		Pseudo-first-order			Pseudo-second-order		
Metals	$q_{e,exp}$ (mg·g^{-1})	$q_{e,cal}$ (mg·g^{-1})	k_1 (min^{-1})	R^2	$q_{e,cal}$ (mg·g^{-1})	k_2 (g·mg^{-1}·min^{-1})	R^2
	Fe_3O_4@ZIF-8						
Cd(II)	27.2	25.5	0.24	0.959	27.9	0.118	0.997
Pb(II)	37.1	36.1	0.53	0.983	37.7	0.087	0.995
	Fe_3O_4@UiO-66–NH_2						
Cd(II)	34.8	31.1	1.83	0.928	35.1	0.075	0.995
Pb(II)	39.5	37.8	1.29	0.953	39.8	0.044	0.993

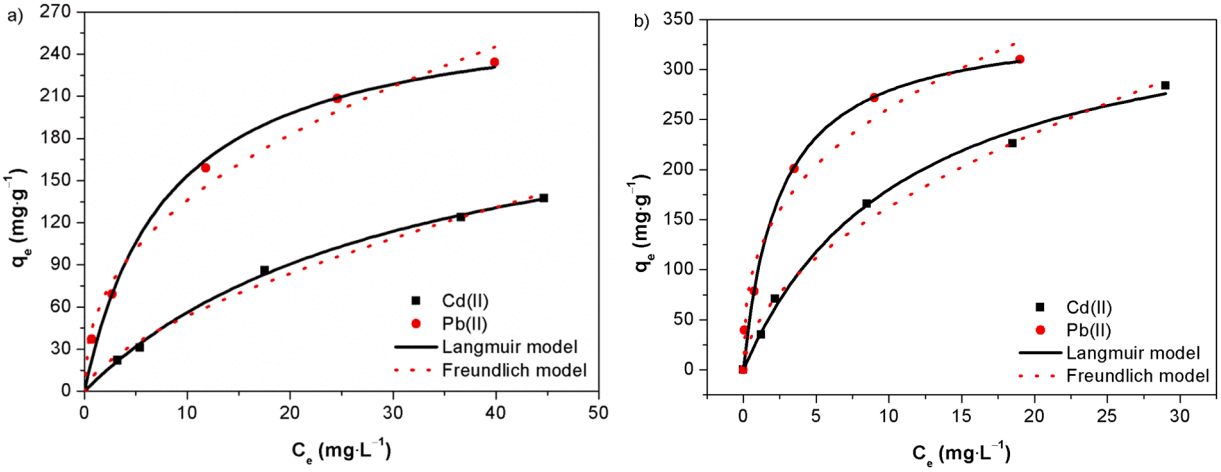

Fig. 5. Langmuir (–) and Freundlich (–) isotherm curves for the adsorption of Cd(II) and Pb(II) using (a) Fe_3O_4@ZIF-8, and (b) Fe_3O_4@UiO-66−NH_2. Experimental conditions: C_0 = (10–100 mg·L^{-1}), Fe_3O_4@ZIF-8 and Fe_3O_4@UiO-66–NH_2 = 2.5 mg, V = 10 mL, time = 8 h, pH = 6 at room temperature.

Fe_3O_4@ZIF-8, and Fe_3O_4@UiO-66–NH_2 nanocomposites, two kinetic models, the pseudo-first-order and the pseudo-second-order models, were fitted to the experimental data (Fig. 4, Fig. S7(c) and (d)), according to Eqs. (3) and (4), respectively.

$$q_t = q_e\left(1 - e^{-k_1 t}\right) \quad (3)$$

$$q_t = \frac{k_2 q_e^2 t}{1 + k_2 q_e t} \quad (4)$$

where k_1 (min^{-1}) and k_2 (g·mg^{-1}·min) are the pseudo-first order and pseudo-second order rate constants of adsorption and q_t (mg·g^{-1}) is the adsorption capacity at a given time t. The calculated kinetic parameters are listed in Table 1.

Adsorption of Cd(II) and Pb(II) using Fe_3O_4@ZIF-8 and Fe_3O_4@UiO-66–NH_2 follows the pseudo-second order model, since the non-linear regression correlations (R^2) were higher than those obtained from the pseudo-first-order model. In addition, the calculated $q_{e,cal}$ values obtained from the pseudo-second order model are much closer to the experimental $q_{e,exp}$, which further demonstrate that the pseudo-second order model is more appropriate for describing the adsorption process using Fe_3O_4@ZIF-8 and Fe_3O_4@UiO-66–NH_2, suggesting that the rate limiting step in governed by surface adsorption [13,14,20].

Table 2
Parameters of Langmuir and Freundlich isotherm models for Cd(II) and Pb(II) adsorption using Fe_3O_4@ZIF-8 and Fe_3O_4@UiO-66–NH_2.

Metals	Langmuir model			Freundlich model		
	$q_{max,cal}$ ($mg{\cdot}g^{-1}$)	K_L ($L{\cdot}g^{-1}$)	R^2	n	K_f ($mg{\cdot}g^{-1}$) ($L{\cdot}g^{-1}$)^n	R^2
	Fe_3O_4@ZIF-8					
Cd(II)	370	6.30	0.998	1.55	12.21	0.989
Pb(II)	666.7	5.89	0.993	2.35	51.17	0986
	Fe_3O_4@UiO-66–NH_2					
Cd(II)	714.3	5.0	0.995	1.85	46.93	0.987
Pb(II)	833.3	5.55	0.990	2.82	115.6	0.971

3.4. Adsorption isotherms

The adsorption capacities of Cd(II) and Pb(II) using Fe_3O_4@ZIF-8, and Fe_3O_4@UiO-66–NH_2 are shown in Fig. 5(a) and (b), respectively. The adsorbed amount of Cd(II) and Pb(II) onto Fe_3O_4@ZIF-8 and Fe_3O_4@UiO-66–NH_2 at equilibrium increase gradually with increasing initial concentrations of the ions, then reaching a plateau where after the respective maximum adsorption capacity under the applied conditions are reached.

The obtained data for the adsorption of Cd(II) and Pb(II) onto Fe_3O_4@ZIF-8 and Fe_3O_4@UiO-66–NH_2 were analyzed using two different isothermal adsorption models, namely Langmuir isotherm and Freundlich isotherm models, respectively (Fig. 5). The calculated adsorption coefficients and the nonlinear regression coefficient (R^2) values for each model are shown in Table 2. The nonlinear Langmuir and Freundlich isotherm models can be described as shown in Eqs. (5) and (6).

$$q_e = \frac{q_{max}\ K_L C_e}{1 + K_L\ C_e} \tag{5}$$

$$q_e = K_f C_e^{1/n} \tag{6}$$

where q_{max} ($mg{\cdot}g^{-1}$) is the maximum adsorption capacity, k_L ($L{\cdot}mg^{-1}$) is the Langmuir equilibrium constant, K_f ($mg^{1-n}{\cdot}L^n{\cdot}g^{-1}$) and n are constants for given adsorbate and adsorbent at a particular temperature.

The correlation coefficient (R^2) values of the Langmuir isotherm model are higher than that of the Freundlich isotherm model, suggesting that a monolayer of Cd(II) and Pb(II) is formed in the adsorption onto Fe_3O_4@ZIF-8 and Fe_3O_4@UiO-66–NH_2 respectively. The maximum adsorption capacities (q_{max}) for Cd(II) and Pb(II) onto Fe_3O_4@ZIF-8 calculated from the Langmuir isotherm model are 370 and 666.7 $mg{\cdot}g^{-1}$, respectively. For Fe_3O_4@UiO-66–NH, a q_{max} of 714.3 and 833.3 $mg{\cdot}g^{-1}$ for adsorption of Cd(II) and Pb(II) respectively, were obtained.

3.5. Adsorption thermodynamics

The adsorption capacities for Cd(II) and Pb(II) at different temperatures are represented in Fig. S8. The q_e values increased with increasing the adsorption temperature due to the higher energy of the system, facilitating the adsorption process, and thus, the adsorption of Cd(II) and Pb(II) are endothermic processes.

The change in q_e as a function of temperature allow us to determine the thermodynamic parameters (enthalpy change ($\Delta H°$), entropy change ($\Delta S°$) and standard free energy ($\Delta G°$)) of the adsorption process using Eqs. 7 and 8.

$$\ln K_d = -\frac{\Delta H°}{RT} + \frac{\Delta S°}{R} \tag{7}$$

$$\Delta G° = \Delta H° - T\Delta S° \tag{8}$$

where R is the universal gas constant (8.314 $J{\cdot}mol^{-1}{\cdot}K^{-1}$), and T (K) is the absolute temperature, and K_d is the equilibrium constant.

When using Van't Hoff's equation for calculating the thermodynamics parameters, a very important remark is that K_d must be dimensionless. Thus, the Langmuir constant, k_L, was corrected according to Eq. 9 to adjust K_e [40,41] (Fig. 6, and Table 3).

$$K_d(dimensionless) = \frac{k_L \times M_a \times M_0 \times 10^3}{\gamma_e} \tag{9}$$

where k_L ($L{\cdot}mg^{-1}$) is the Langmuir equilibrium constant, M_a ($g{\cdot}mol^{-1}$) is the molar mass of adsorbate, M_0 ($mol{\cdot}L^{-1}$) is the standard concentration of adsorbate (usually used as 1.0 $mol{\cdot}L^{-1}$ for diluted solutions), γ_e is the chemical activity of the adsorbate (which can be assumed to be 1.0 for dilute solutions).

The calculated values of $\Delta G°$ at each temperature are negative, suggesting that the adsorption processes of Cd(II) and Pb(II) are spontaneous. For $\Delta H°$ the values are positive, in combination with the fact that the adsorption capacities of Cd(II) and Pb(II) increases with increasing the temperature, this demonstrates that the adsorption process is endothermic. In addition, the positive values of $\Delta S°$ indicates that the adsorption of Cd(II) and Pb(II) using Fe_3O_4@ZIF-8 and Fe_3O_4@UiO-66–NH_2 is entropy driven, and rising the temperature will increase the

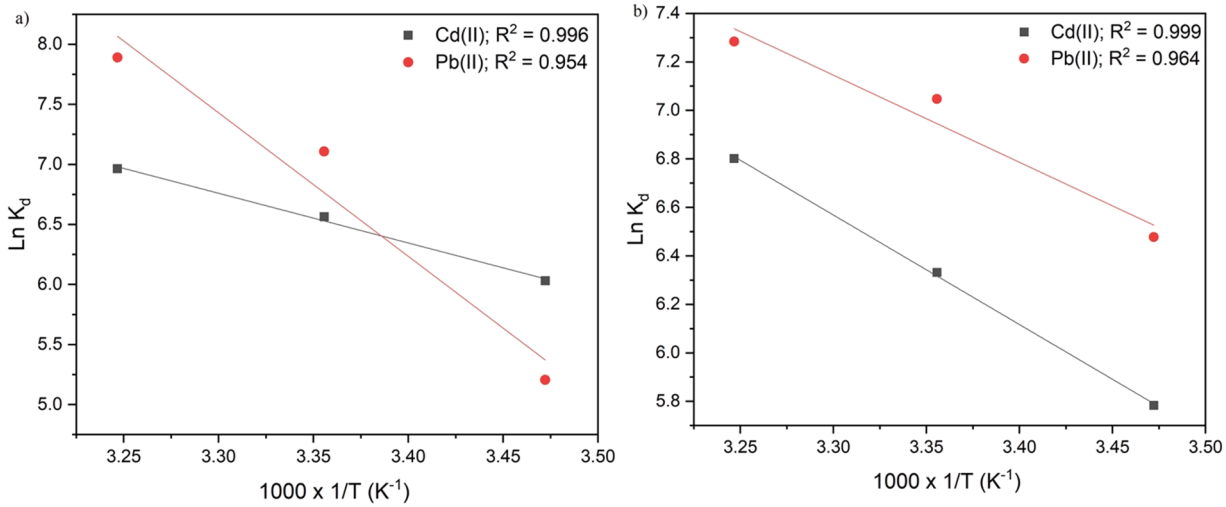

Fig. 6. Linear plot of ln K_d vs. 1/T for the adsorption of Cd(II) and Pb(II) using (a)Fe_3O_4@ZIF-8 and (b) Fe_3O_4@UiO-66–NH_2. Experimental conditions: C_0 = 10 $mg{\cdot}L^{-1}$, Fe_3O_4@ZIF-8 and Fe_3O_4@UiO-66–NH_2 = 2.5 mg, V = 10 mL, pH = 6, and t = 8 h.

Table 3
Thermodynamic parameters for the adsorption of Cd(II) and Pb(II) using Fe_3O_4@ZIF-8 and Fe_3O_4@UiO-66–NH_2.

Adsorbate	T (K)	K_L ($L{\cdot}g^{-1}$)	K_d	ln K_d	ΔG^o ($kJ{\cdot}mol^{-1}$)	ΔH^o ($kJ{\cdot}mol^{-1}$)	ΔS^o ($J{\cdot}mol^{-1}{\cdot}k^{-1}$)
Fe_3O_4@ZIF-8							
Cd(II)	288	3.7	415.9318	6.0305	–14.44	34.42	169.8
	298	6.3	708.2082	6.5627	–16.26		
	308	9.4	1056.6916	6.9628	–17.83		
Pb(II)	288	0.88	182.336	5.2058	–12.46	96.35	389.7
	298	5.89	1220.408	7.1069	–17.61		
	308	12.89	2671.104	7.8902	–20.20		
Fe_3O_4@UiO-66–NH_2							
Cd(II)	288	2.89	324.876	5.7834	–13.84	37.56	178.5
	298	5.0	562.07	6.3316	–15.68		
	308	8.0	899.312	6.8016	–17.42		
Pb(II)	288	3.13	650.039	6.4770	–15.50	29.88	158.0
	298	5.55	1149.960	7.0477	–17.46		
	308	7.03	1456.8457	7.2840	–22.43		

Table 4
Cd(II) and Pb(II) removal percentages using Fe_3O_4@ZIF-8 and Fe_3O_4@UiO-66–NH_2 in the presence of Ca(II) and Mg(II) as competing cations.

Metals	Removal% at various concentrations of Ca (II) and Mg (II)[a]		
	0	10 $mg{\cdot}L^{-1}$	50 $mg{\cdot}L^{-1}$
Fe_3O_4@ZIF-8			
Cd(II)	67	64	64
Pb(II)	94	89	90
Fe_3O_4@UiO-66-NH_2			
Cd(II)	88	85	85
Pb(II)	99	97	97

[a]Experiment conditions: Cd(II) = 10 $mg{\cdot}L^{-1}$, Pb(II) = 10 $mg{\cdot}L^{-1}$, Adsorbent = 2.5 mg, v = 10 mL, t = 8 h, at pH 6.0.

disorder of the whole system.

3.6. Effect of competing cations

Alkaline divalent cations including Ca(II) and Mg(II) exist in wastewater and natural water in high concentrations and may compete with toxic heavy metal ions for the available binding sites of the adsorbent materials. Therefore, evaluating the adsorption of Cd(II) and Pb(II) in the presence of other competing cations such as Ca(II) and Mg (II) using Fe_3O_4@ZIF-8 and Fe_3O_4@UiO-66–NH_2 at various concentrations were assessed. As can be seen from the tabulated results in Table 4, the removal efficiencies of Cd(II) and Pb(II) using Fe_3O_4@ZIF-8 and Fe_3O_4@UiO-66–NH_2 were slightly influenced by adding Ca(II) and Mg (II) as competing cations. Thus, Fe_3O_4@ZIF-8 and Fe_3O_4@UiO-66–NH_2 are promising adsorbents for the removal of Cd(II) and Pb(II) from aqueous solutions, even in the presence of Ca(II), and Mg(II) at high concentrations.

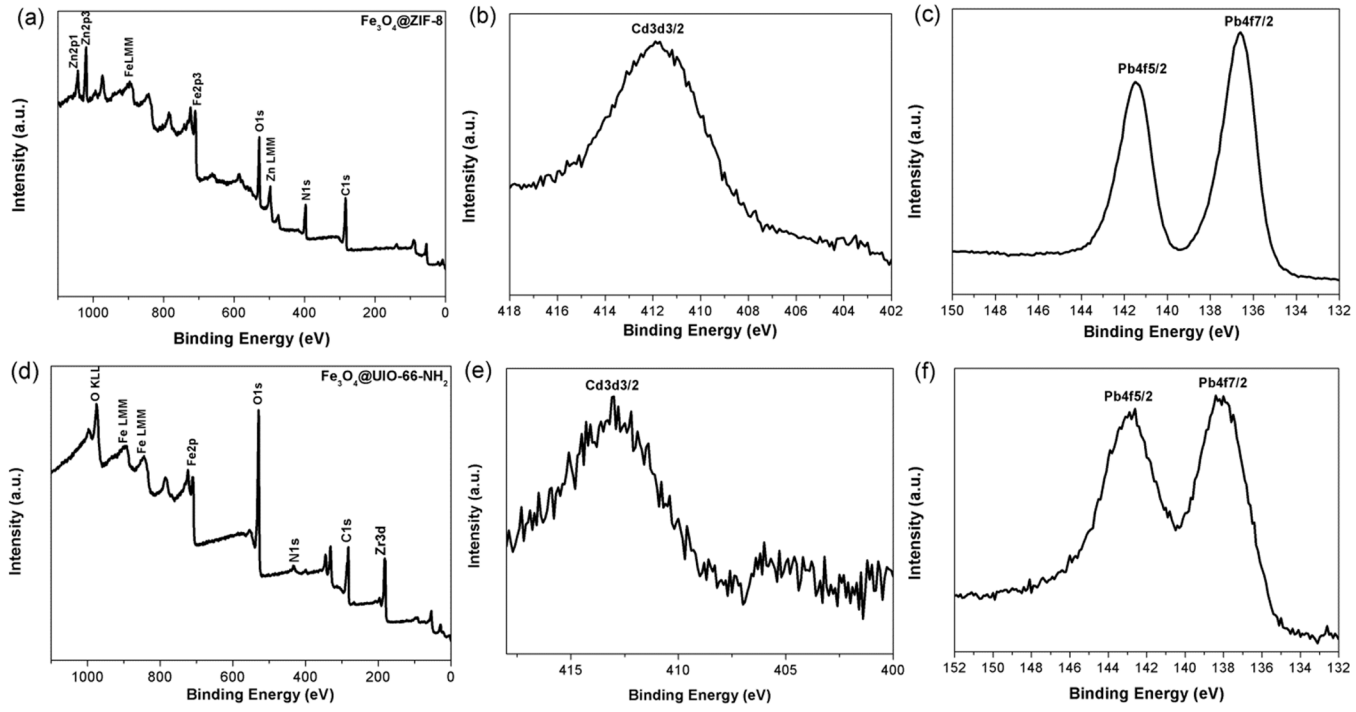

Fig. 7. XPS results of Fe_3O_4@ZIF-8, and Fe_3O_4@UiO-66–NH_2 samples. (a-c) Fe_3O_4@ZIF-8 sample: (a) survey spectrum; (b) high-resolution spectrum of Cd3d after adsorption of Cd(II); (c) high-resolution spectrum of Pb 4 f after the adsorption of Pb(II). (d-f) Fe_3O_4@UiO-66–NH_2 sample: (a) survey spectrum;(e) high-resolution spectrum of Cd3d after adsorption of Cd(II); (f) high-resolution spectrum of Pb 4 f after the adsorption of Pb(II).

Table 5
Comparison of the adsorption of Cd(II) and Pb(II) from aqueous solution using various magnetic adsorbents.

Magnetic adsorbent	q_{max} ($mg \cdot g^{-1}$)		Experimental conditions	Ref.
	Cd (II)	Pb (II)		
Fe_3O_4/[Cu($C_8H_6NO_4$)$_2$]$_n$/L-cysteine	248.2	–	Adsorption: 50 mg Fe_3O_4/MOF/L-cysteine, 200 rpm for 20 min Desorption: 1.0 mL 1 $mol \cdot L^{-1}$ HCl was added to the used Fe_3O_4/MOF/L-cysteine and the mixture was ultrasonicated for 20 min	[43]
Fe_3O_4@APS@AA-co-CA MNPs	29.6	166.1	Adsorption: adsorbent: 1.0 $g \cdot L^{-1}$, initial concentration of metal ions, 20–450 $mg \cdot L^{-1}$, temperature: 298 K, pH: 5.5, time: 45 min Desorption: 0.050 g metal ion loaded. adsorbents to 50 mL aqueous solution with 0.1 $mol \cdot L^{-1}$ hydrochloric acid. The mixture was shaken for 3 h to reach desorption equilibrium.	[44]
Fe_3O_4@Cu_3(btc)$_2$	–	215	Adsorption: 10 mg of the thiol-functionalized Fe_3O_4@Cu_3(btc)$_2$ was added to 10 mL of the Hg^{2+} and Pb^{2+} mixed metal ions solutions (0.1–1000 $mg \cdot L^{-1}$, under constant shaking at room temperature for 2 h. Desorption: Washing three times with NaOH solution (0.01 M, 5 mL × 3) with sonication for 30 min	[45]
	186	198	Adsorption: adsorbent: 30 mg, initial concentration of metal ions, 20–450 $mg \cdot L^{-1}$, temperature: 298 K, pH = 7.5, time = 16 min Desorption: 6 mL of 0.8 $mol \cdot L^{-1}$ EDTA in 0.01 $mol \cdot L^{-1}$ NaOH solution.	[46]
	188	104	Adsorption: 25 mg of the adsorbent dithizone-modified Fe_3O_4@Cu_3(btc)$_2$, pH = 6.4; contact time 13 min Desorption: 0.01 $mol \cdot L^{-1}$ NaOH in a thiourea solution as the elution solvent.	[47]
Fe_3O_4@ZIF-8	370	666.7	Adsorption: Fe_3O_4@ZIF-8 and Fe_3O_4@UiO-66–NH_2 = 2.5 mg, V = 10 mL, C_0 = 10 $mg \cdot L^{-1}$, pH = 6, and contact time 8 h. Desorption: 10 mL of acetonitrile was added to the loaded Fe_3O_4@ZIF-8 and Fe_3O_4@UiO-66–NH_2 (2.5 mg) and the mixture was stirred for 10 h.	This work
Fe_3O_4@UiO-66–NH_2	714.3	833.3		

APS = 3-aminopropyltriethoxysilane; AA = acrylic acid; CA = crotonic acid; btc = benzene-1,3,5-tricarboxylic acid.

3.7. Proposed adsorption mechanism

Based on the adsorbents, there are several proposed mechanisms for the removal of target metal ions. Complexation with the frameworks, electrostatic interactions, and ion exchange may take place during the adsorption process. To gain further insight into the possible mechanism for the adsorption of Cd(II) and Pb(II) onto Fe_3O_4@ZIF-8 and Fe_3O_4@UiO-66–NH_2, XPS analysis of the MOFs after adsorption were carried out. The XPS survey spectrums demonstrates that peaks of Zn, Fe, O, N, and C are found in Fe_3O_4@ZIF-8 (Fig. 7(a)), while peaks of Zr, Fe, O, N, and C are found in Fe_3O_4@UiO-66–NH_2 (Fig. 7(d)). After adsorption of Cd(II) and Pb(II), the high-resolution XPS spectrum of Fe_3O_4@ZIF-8 shows peaks at binding energies of 412.1 eV (corresponding to Cd $3d^{3/2}$) (Fig. 7(b)), 137.2 and 142.1 eV, (corresponding to Pb 4 $f^{7/2}$, and Pb 4 $f^{5/2}$, respectively) (Fig. 7(c)), indicating that both Cd (II) and Pb(II) were adsorbed to the Fe_3O_4@ZIF-8 sample. For the Fe_3O_4@UiO-66–NH_2 sample, peaks of Cd $3d^{3/2}$, Pb 4 $f^{7/2}$, and Pb 4 $f^{5/2}$ can be found in the high-resolution XPS spectrums of Fe_3O_4@UiO-66–NH_2 after adsorption of Cd(II) and Pb(II). The binding energies of $Pb4f^{7/2}$ and $Pb4f^{5/2}$ in $Pb(NO_3)_2$ are 139.6 eV and 144.5 eV, respectively, while in this study the binding energies of Pb 4 $f^{7/2}$ and Pb 4 $f^{5/2}$ are approximately 137 eV and 142 eV, respectively, in both Fe_3O_4@ZIF-8 and Fe_3O_4@UiO-66–NH_2 samples. Thus, compared with the binding energies of Pb 4 f in $Pb(NO_3)_2$, those of Pb 4 f in Fe_3O_4@ZIF-8 and Fe_3O_4@UiO-66–NH_2 samples significantly shift to lower range (approximately 2 eV shift). This significant binding energies shift of Pb 4 f can be attributed to the formation of strong affinities between Pb(II) and the prepared materials. The energy separation of 4.9 eV and 5.2 eV between the Pb 4 $f^{5/2}$ and 4 $f^{7/2}$ for adsorption onto Fe_3O_4@ZIF-8 and Fe_3O_4@UiO-66–NH_2, respectively, confirmed the coordination interaction between Pb(II) and the adsorbent. The obtained XPS analysis for Fe_3O_4@ZIF-8 and Fe_3O_4@UiO-66–NH_2 before and after the adsorption process, indicates that the used magnetic MOFs in this study can adsorb Cd(II) and Pb(II) via a coordination interaction between Cd(II) and Pb (II) and the imino groups of 2-methylimidazole of the ZIF-8 shell of Fe_3O_4@ZIF-8 [25], and via a coordination interaction between Cd(II) and Pb(II) and the amino group of Fe_3O_4@UiO-66–NH_2 [42]. No extra peaks after the adsorption for the possible formation of new solid phases could be observed by XPS analysis, which demonstrates that the adsorption of Cd(II) and Pb(II) from aqueous solutions using Fe_3O_4@ZIF-8 and Fe_3O_4@UiO-66–NH_2 is mainly attributed to coordination reactions.

3.8. Recycling and desorption studies

To evaluate the potential reusability of the synthesized magnetic Fe_3O_4@ZIF-8 and Fe_3O_4@UiO-66–NH_2 composites for Cd(II) and Pb(II) removal, the regeneration process was carried out using acetonitrile solution for 10 h. As shown in Fig. S9, after four-cycles of regeneration, the Fe_3O_4@ZIF-8 and Fe_3O_4@UiO-66–NH_2 still exhibits almost the same initial removal percentage, indicating the good recycling ability of Fe_3O_4@ZIF-8, and Fe_3O_4@UiO-66–NH_2. The results confirmed the high stability and reusability of the synthesized magnetic Fe_3O_4@ZIF-8 and Fe_3O_4@UiO-66–NH_2 adsorbents.

3.9. Comparison with other adsorbents

The q_{max} determined in this study for adsorption of Cd(II) and Pb(II) onto both Fe_3O_4@ZIF-8 and Fe_3O_4@UiO-66$-NH_2$, compare well with other MOFs lacking MNPs (Table 5). However, the composite magnetic materials investigated in the present study can be separated easily from aqueous solutions using an external magnet, which is favorable for industrial implementation. Furthermore, no extra reagents is required during adsorption [43]. The adsorption and desorption conditions are simple and can be easily scaled-up. Magnetic MOFs show high performance compared to various materials such as Fe_3O_4 magnetic nanoparticles modified with 3-aminopropyltriethoxysilane (APS) and copolymers of acrylic acid (AA) and crotonic acid (CA) [44], and Fe_3O_4@Cu_3(btc)$_2$ [45].

4. Conclusions

In this work, two magnetically-separable metal-organic frameworks, Fe_3O_4@ZIF-8, and Fe_3O_4@UiO-66–NH_2, have been synthesized and fully characterized. The magnetic Fe_3O_4@ZIF-8, and Fe_3O_4@UiO-

66–NH_2 exhibits excellent adsorption performance for Cd(II) and Pb(II) removal from aqueous solutions. In addition, the Fe_3O_4@ZIF-8, and Fe_3O_4@UiO-66–NH_2 adsorbent showed excellent reusability, being highly efficient and effective after at least four consecutive adsorption-desorption cycles, indicating its impact for the removal of hazardous metal ions from aqueous solutions. Mechanism investigation revealed that coordination reactions were the main mechanisms involved in the removal of Cd(II) and Pb(II) by Fe_3O_4@ZIF-8, and Fe_3O_4@UiO-66–NH_2 from aqueous solution. Thus, our results may pave a way for developing an easily separable adsorbents for efficient removal of Cd(II) and Pb(II) from aqueous solutions.

CRediT authorship contribution statement

Ahmed F. Abdel-Magied: Conceptualization, Methodology, Supervision, Investigation, Writing – review & editing. **Hani Nasser Abdelhamid**: Conceptualization, Methodology, Supervision, Investigation, Writing – review & editing, Funding acquisition. **Radwa M. Ashour**: Methodology, Investigation. **Le Fu**: Investigation. **Moataz Dowaidar**: Investigation. **Wei Xia**: Methodology, Supervision. **Kerstin Forsberg**: Conceptualization, Methodology, Supervision, Investigation, Writing – review & editing, Funding acquisition.

Declaration of Competing Interest

The authors declare that they have no known competing financial interests or personal relationships that could have appeared to influence the work reported in this paper.

Acknowledgments

This work was supported by the Swedish Research Council (VR), and the Swedish Governmental Agency for Innovation Systems (VINNOVA) via Prof. X. Zou whoprovided part of the necessary tools to do these measurements in her lab at SU, Sweden. H.N. Abdelhamid thanks Science, Technology & Innovation Funding Authority (STDF, Project ID 35969, Egypt) for the support.

References

[1] M.T. Lucas, T.G. Noordewier, Environmental management practices and firm financial performance: the moderating effect of industry pollution-related factors, Int. J. Prod. Econ. 175 (2016) 24–34.
[2] Z. Wan, M. Zhu, S. Chen, D. Sperling, Pollution: Three steps to a green shipping industry, Nature 530 (2016) 275–277.
[3] B. Gworek, W. Dmuchowski, E. Koda, M. Marecka, A.H. Baczewska, P. Brągoszewska, A. Sieczka, P. Osiński, Impact of the municipal solid waste łubna landfill on environmental pollution by heavy metals, Water 8 (2016) 470.
[4] H. Shahriyari Far, M. Hasanzadeh, M. Najafi, T.R. Masale Nezhad, M. Rabbani, Efficient removal of Pb(II) and Co(II) Ions from aqueous solution with a chromium-based metal–organic framework/activated carbon composites, Ind. Eng. Chem. Res. 60 (2021) 4332–4341.
[5] G. Genchi, M.S. Sinicropi, G. Lauria, A. Carocci, A. Catalano, The effects of cadmium toxicity, Int. J. Environ. Res. Public Health 17 (2020) 3782.
[6] H.-J. Tsai, P.-Y. Wu, J.-C. Huang, S.-C. Chen, Environmental pollution and chronic kidney disease, Int. J. Med. Sci. 18 (2021) 1121–1129.
[7] J.O. Esalah, M.E. Weber, J.H. Vera, Removal of lead, cadmium and zinc from aqueous solutions by precipitation with sodium Di-(n-octyl) phosphinate, Can. J. Chem. Eng. 78 (2000) 948–954.
[8] M. Aliabadi, M. Irani, J. Ismaeili, H. Piri, M.J. Parnian, Electrospun nanofiber membrane of PEO/Chitosan for the adsorption of nickel, cadmium, lead and copper ions from aqueous solution, Chem. Eng. J. 220 (2013) 237–243.
[9] S. Ahmed, S. Chughtai, M.A. Keane, The removal of cadmium and lead from aqueous solution by ion exchange with Na•Y zeolite, Sep. Purif. Technol. 13 (1998) 57–64.
[10] Y. Yuan, Y. Wu, H. Wang, Y. Tong, X. Sheng, Y. Sun, X. Zhou, Q. Zhou, Simultaneous enrichment and determination of cadmium and mercury ions using magnetic PAMAM dendrimers as the adsorbents for magnetic solid phase extraction coupled with high performance liquid chromatography, J. Hazard. Mater. 386 (2020), 121658.
[11] A.O. Bello, B.S. Tawabini, A.B. Khalil, C.R. Boland, T.A. Saleh, Phytoremediation of cadmium-, lead- and nickel-contaminated water by Phragmites australis in hydroponic systems, Ecol. Eng. 120 (2018) 126–133.
[12] J.E.D.V. Segundo, G.R. Salazar-Banda, A.C.O. Feitoza, E.O. Vilar, E.B. Cavalcanti, Cadmium and lead removal from aqueous synthetic wastes utilizing Chemelec electrochemical reactor: Study of the operating conditions, Sep. Purif. Technol. 88 (2012) 107–115.
[13] R.M. Ashour, R. El-sayed, A.F. Abdel-Magied, A.A. Abdel-khalek, M.M. Ali, K. Forsberg, A. Uheida, M. Muhammed, J. Dutta, Selective separation of rare earth ions from aqueous solution using functionalized magnetite nanoparticles: kinetic and thermodynamic studies, Chem. Eng. J. 327 (2017) 286–296.
[14] R.M. Ashour, H.N. Abdelhamid, A.F. Abdel-Magied, A.A. Abdel-Khalek, M.M. Ali, A. Uheida, M. Muhammed, X. Zou, J. Dutta, Rare earth ions adsorption onto graphene oxide nanosheets, Solvent Extr. Ion. Exch. 35 (2017) 91–103.
[15] S. Tong, H. Deng, L. Wang, T. Huang, S. Liu, J. Wang, Multi-functional nanohybrid of ultrathin molybdenum disulfide nanosheets decorated with cerium oxide nanoparticles for preferential uptake of lead (II) ions, Chem. Eng. J. 335 (2018) 22–31.
[16] N.E.-A. El-Naggar, R.A. Hamouda, I.E. Mousa, M.S. Abdel-Hamid, N.H. Rabei, Statistical optimization for cadmium removal using Ulva fasciata biomass: characterization, immobilization and application for almost-complete cadmium removal from aqueous solutions, Sci. Rep. 8 (2018) 12456.
[17] J. Hong, J. Xie, S. Mirshahghassemi, J. Lead, Metal (Cd, Cr, Ni, Pb) removal from environmentally relevant waters using polyvinylpyrrolidone-coated magnetite nanoparticles, RSC Adv. 10 (2020) 3266–3276.
[18] H. Zhu, X. Tan, L. Tan, H. Zhang, H. Liu, M. Fang, T. Hayat, X. Wang, Magnetic porous polymers prepared via high internal phase emulsions for efficient removal of Pb2+ and Cd2+, ACS Sustain. Chem. Eng. 6 (2018) 5206–5213.
[19] F. Lu, D. Astruc, Nanomaterials for removal of toxic elements from water, Coord. Chem. Rev. 356 (2018) 147–164.
[20] A.F. Abdel-Magied, H.N. Abdelhamid, R.M. Ashour, X. Zou, K. Forsberg, Hierarchical porous zeolitic imidazolate frameworks nanoparticles for efficient adsorption of rare-earth elements, Microporous Mesoporous Mater. 278 (2019) 175–184.
[21] P.A. Kobielska, A.J. Howarth, O.K. Farha, S. Nayak, Metal–organic frameworks for heavy metal removal from water, Coord. Chem. Rev. 358 (2018) 92–107.
[22] M. Feng, P. Zhang, H.-C. Zhou, V.K. Sharma, Water-stable metal-organic frameworks for aqueous removal of heavy metals and radionuclides: a review, Chemosphere 209 (2018) 783–800.
[23] R.M. Ashour, A.F. Abdel-Magied, Q. Wu, R.T. Olsson, K. Forsberg, Green synthesis of metal-organic framework bacterial cellulose nanocomposites for separation applications, Polymers 12 (2020).
[24] R. Ricco, L. Malfatti, M. Takahashi, A.J. Hill, P. Falcaro, Applications of magnetic metal–organic framework composites, J. Mater. Chem. A. 1 (2013) 13033–13045.
[25] X. Jiang, S. Su, J. Rao, S. Li, T. Lei, H. Bai, S. Wang, X. Yang, Magnetic metal-organic framework (Fe3O4@ZIF-8) core-shell composite for the efficient removal of Pb(II) and Cu(II) from water, J. Environ. Chem. Eng. 9 (2021), 105959.
[26] W. Guo, Z. Zhang, P. Chen, X. Luan, J. Dou, J. Bai, H. Fang, W. Shi, B. Zhou, CMP-on-MOF bimetallic hybrids derived sheet-on-rod heterostructure as bifunctional oxygen electrocatalyst for rechargeable Zn-air batteries, Microporous Mesoporous Mater. 331 (2022), 111639.
[27] K.S. Park, Z. Ni, A.P. Côté, J.Y. Choi, R. Huang, F.J. Uribe-Romo, H.K. Chae, M. O'Keeffe, O.M. Yaghi, Exceptional chemical and thermal stability of zeolitic imidazolate frameworks, PNAS 103 (2006) 10186.
[28] J.H. Cavka, S. Jakobsen, U. Olsbye, N. Guillou, C. Lamberti, S. Bordiga, K. P. Lillerud, A. New, Zirconium inorganic building brick forming metal organic frameworks with exceptional stability, J. Am. Chem. Soc. 130 (2008) 13850–13851.
[29] M. Dowaidar, H. Nasser Abdelhamid, M. Hällbrink, Ü. Langel, X. Zou, Chitosan enhances gene delivery of oligonucleotide complexes with magnetic nanoparticles-cell-penetrating peptide, J. Biomater. Appl. 33 (2018) 392–401.
[30] H.N. Abdelhamid, Y.C. Lin, H.-F. Wu, Magnetic nanoparticle modified chitosan for surface enhanced laser desorption/ionization mass spectrometry of surfactants, RSC Adv. 7 (2017) 41585–41592.
[31] J. Gopal, H.N. Abdelhamid, P.-Y. Hua, H.-F. Wu, Chitosan nanomagnets for effective extraction and sensitive mass spectrometric detection of pathogenic bacterial endotoxin from human urine, J. Mater. Chem. B 1 (2013) 2463–2475.
[32] C. Zhang, Y. Zhao, Y. Li, X. Zhang, L. Chi, G. Lu, Defect-controlled preparation of UiO-66 metal-organic framework thin films with molecular sieving capability, Chem. Asian J. 11 (2016) 207–210.
[33] H.N. Abdelhamid, Z. Huang, A.M. El-Zohry, H. Zheng, X. Zou, A fast and scalable approach for synthesis of hierarchical porous zeolitic imidazolate frameworks and one-pot encapsulation of target molecules, Inorg. Chem. 56 (2017) 9139–9146.
[34] J. Landers, G.Y. Gor, A.V. Neimark, Density functional theory methods for characterization of porous materials, Colloids Surf. A Physicochem. Eng. Asp. 437 (2013) 3–32.
[35] H.N. Abdelhamid, A.P. Mathew, Cellulose-zeolitic imidazolate frameworks (CelloZIFs) for multifunctional environmental remediation: adsorption and catalytic degradation, Chem. Eng. J. 426 (2021), 131733.
[36] H.N. Abdelhamid, A.P. Mathew, In-situ growth of zeolitic imidazolate frameworks into a cellulosic filter paper for the reduction of 4-nitrophenol, Carbohydr. Polym. 274 (2021), 118657.
[37] R. Laus, T.G. Costa, B. Szpoganicz, V.T. Fávere, Adsorption and desorption of Cu (II), Cd(II) and Pb(II) ions using chitosan crosslinked with epichlorohydrin-triphosphate as the adsorbent, J. Hazard. Mater. 183 (2010) 233–241.
[38] G. Zeng, Y. Liu, L. Tang, G. Yang, Y. Pang, Y. Zhang, Y. Zhou, Z. Li, M. Li, M. Lai, X. He, Y. He, Enhancement of Cd(II) adsorption by polyacrylic acid modified magnetic mesoporous carbon, Chem. Eng. J. 259 (2015) 153–160.

[39] N. Yin, K. Wang, Ya Xia, Z. Li, Novel melamine modified metal-organic frameworks for remarkably high removal of heavy metal Pb (II), Desalination 430 (2018) 120–127.
[40] E.C. Lima, A. Hosseini-Bandegharaei, J.C. Moreno-Piraján, I. Anastopoulos, A critical review of the estimation of the thermodynamic parameters on adsorption equilibria. Wrong use of equilibrium constant in the Van't Hoof equation for calculation of thermodynamic parameters of adsorption, J. Mol. Liq. 273 (2019) 425–434.
[41] Y. Liu, Is the free energy change of adsorption correctly calculated? J. Chem. Eng. Data 54 (2009) 1981–1985.
[42] K. Wang, J. Gu, N. Yin, Efficient removal of Pb(II) and Cd(II) using NH2-functionalized Zr-MOFs via rapid microwave-promoted synthesis, Ind. Eng. Chem. Res. 56 (2017) 1880–1887.
[43] L. Fan, M. Deng, C. Lin, C. Xu, Y. Liu, Z. Shi, Y. Wang, Z. Xu, L. Li, M. He, A multifunctional composite Fe3O4/MOF/l-cysteine for removal, magnetic solid phase extraction and fluorescence sensing of Cd(ii), RSC Adv. 8 (2018) 10561–10572.
[44] F. Ge, M.-M. Li, H. Ye, B.-X. Zhao, Effective removal of heavy metal ions Cd2+, Zn2+, Pb2+, Cu2+ from aqueous solution by polymer-modified magnetic nanoparticles, J. Hazard. Mater. 211–212 (2012) 366–372.
[45] F. Ke, J. Jiang, Y. Li, J. Liang, X. Wan, S. Ko, Highly selective removal of Hg2+ and Pb2+ by thiol-functionalized Fe3O4@metal-organic framework core-shell magnetic microspheres, Appl. Surf. Sci. 413 (2017) 266–274.
[46] M.R. Sohrabi, Z. Matbouie, A.A. Asgharinezhad, A. Dehghani, Solid phase extraction of Cd(II) and Pb(II) using a magnetic metal-organic framework, and their determination by FAAS, Microchim. Acta 180 (2013) 589–597.
[47] M. Taghizadeh, A.A. Asgharinezhad, M. Pooladi, M. Barzin, A. Abbaszadeh, A. Tadjarodi, A novel magnetic metal organic framework nanocomposite for extraction and preconcentration of heavy metal ions, and its optimization via experimental design methodology, Microchim. Acta 180 (2013) 1073–1084.